Supplementary Materials for

Intrinsic properties of human germinal-center B cells set antigen-affinity thresholds

Kihyuck Kwak, Nicolas Quizon, Haewon Sohn, Avva Saniee, Javier Manzella-Lapeira, Prasida Holla, Joseph Brzostowski, Jinghua Lu, HengYi Xie, Chenguang Xu, Katelyn M. Spillane, Pavel Tolar[4,5] and Susan K. Pierce[*]

Corresponding author. Email: spierce@nih.gov

The PDF file includes:

Movie S2. The dynamics of membrane movement in the immune synapse upon activation were visualized by IRM.

Movie S3. Time-lapse imaging of CD19 and BCR in the immune synapse of naïve B cells and LZ GC B cells.

Movie S4. Pulling forces in the immune synapse of live naïve and LZ GC B cells were monitored with time using DNA-based force sensors.

Movie S5. Colocalization of the cell contact sites and the locations of pulling force in LZ GC B cell.

Movie S6. The dynamics of membrane movement in the immune synapse of naïve and LZ GC B cell upon activation by high- or low-affinity antigen were visualized by DIC and IRM.

Movie S7. Motile LZ GC B cells were observed upon activation by low-affinity antigen.

Movie S8. Distinct antigen transport pattern shown in human LZ GC B cells on PMS presenting surrogate antigens as compared to naïve B cells.

Movie S9. Localization of MTOC with SNX9 or SNX18 after activation in naïve and LZ GC B cells.

Movie S10. Localization of LAMP-1 after activation in naïve and LZ GC B cells.

Other Supplementary Material for this manuscript includes the following:

Table S1 (Microsoft Excel format). Raw data file

Methods

Purification and sorting of human tonsillar B lymphocytes

Tonsils were obtained from patients undergoing tonsillectomies. The tonsillar tissue was cut into small pieces, and cells were harvested in media containing RPMI medium 1640, 10% FBS, sodium pyruvate, L-glutamine, non-essential amino acids, Penn-strep, HEPES, and beta-mercaptoethanol (RPMI-10) with gentle tapping. The tonsillar cells were then filtered through cell strainers with 70 micron pores to obtain single cell-suspensions. Tonsillar B cells were isolated by negative selection using the EasySep Human B cell enrichment kit (STEMCELL) and, when required, were further sorted using DyLight 405 (Innova Biosciences) conjugated anti-IgD Fab (SouthernBiotech), BV786 anti-CD10 (BD Biosciences), PE anti-CD184 (BD Biosciences), and DyLight 488 (Innova Biosciences) conjugated anti-λlight chain Fab (SouthernBiotech) with a FACSAria II cell sorter (BD Biosciences).

TIRF microscopy

Sorted cells were stained with either Alexa Fluor 488 or Alexa Fluor 647 anti-IgM Fab antibodies (Jackson ImmunoResearch) for naïve and IgM GC B cells or Alexa Fluor 488 or Alexa Fluor 647 anti-IgG Fab antibodies (Jackson ImmunoResearch) for IgG GC B cells, placed on PLB presenting goat $F(ab')_2$ anti-human Igκ (SouthernBiotech) and anti-human Igλ (SouthernBiotech) surrogate antigens or without antigen. They were then incubated at 37°C for the times indicated, fixed in 4% PFA, permeabilized in saponin, and stained with either pSyk-specific antibodies (Cell Signaling), Alexa Fluor 647 labeled pPLCγ2-specific antibodies (BD Biosciences), pPI3K-specific antibodies (Cell Signaling), pBtk-specific antibodies (Cell Signaling), DyLight 650 (Innova Biosciences) conjugated pVav-specific antibodies (Abcam),

DyLight 488 (Innova Biosciences) conjugated pCbl-specific antibodies (Santa Cruz Biotechnology), or pSHP-1-specific antibodies (Cell Signaling). For cells stained with primary antibodies, Alexa Fluor 488 secondary antibodies (Invitrogen) were used as detecting reagents. Images were acquired by Olympus IX-81 TIRF microscope system. To analyze the levels of phosphorylated signaling molecules, MFI values of pSyk, pPLCγ2, pPI3K, pBtk, pVav, pCbl, or pSHP-1 within the immune synapse were analyzed by MatLab (MathWorks) software. The Pearson's correlation coefficients of signaling molecules and BCR were calculated from background-subtracted images by MatLab (MathWorks).

Time-lapse live cell TIRF imaging was done at 37°C on a climate-controlled stage with 5% CO_2 and 75% humidity. Naïve B cells were stained with Alexa Fluor 647 anti-IgM Fab (Jackson ImmunoResearch) and DyLight 488 (Innova Biosciences) conjugated anti-CD19 (Biolegend) Fab while LZ GC and DZ GC B cells were stained with Alexa Fluor 647 anti-IgG Fab (Jackson ImmunoResearch) and DyLight 488 (Innova Biosciences) conjugated anti-CD19 (Biolegend) Fab. Each B cell subset was placed on PLBs containing goat $F(ab')_2$ anti-human Igκ (SouthernBiotech) and anti-human Igλ (SouthernBiotech) surrogate antigen and TIRF images were acquired at 6 sec intervals for 20 min. The Pearson's correlation coefficient (R) of CD19 and BCR were calculated from background-subtracted images by MatLab (Mathworks). For time-lapse live cell DIC and IRM TIRF imaging, naïve and LZ GC B cells were placed on PLB presenting Alexa 647 goat $F(ab')_2$ anti-human Igκ (SouthernBiotech) and anti-human Igλ (SouthernBiotech) surrogate antigens or without antigen and incubated at 37°C on a climate-controlled stage with 5% CO_2 and 75% humidity, and TIRF images were acquired at 3 sec intervals for 15 min after activation.

For the affinity discrimination experiment using high and low-affinity antigen, Igκ$^+$ naïve and LZ GC B cells were stained with DyLight 488 anti-IgM Fab (Jackson ImmunoResearch) for naïve B cells or DyLight 488 anti-IgG Fab (Jackson ImmunoResearch) for GC B cells, placed on PLBs either presenting anti-human Igκ, anti- rat Igκ antibodies, or without antigen. They were then incubated at 37°C for the times indicated in the figure legends, fixed in 4% PFA, permeabilized with saponin, and stained with anti-pCD79A (Cell Signaling), anti-pSyk (Cell Signaling), Alexa Fluor 647 anti-pBLNK (BD Biosciences), or Alexa Fluor 647 anti-pPLCγ2 (BD Biosciences). Primary anti-pCD79A (Cell Signaling), anti-pSyk (Cell Signaling) antibodies were labeled with Alexa Fluor 647 secondary antibodies (Invitrogen) for cell staining. For time-lapse live cell imaging, Igκ$^+$ naïve and LZ GC B cells were placed on PLB presenting anti-human Igκ or anti- rat Igκ antibodies surrogate antigens and incubated at 37°C on a climate-controlled stage with 5% CO_2 and 75% humidity, and DIC and IRM images were acquired at 3 sec intervals for 15 min. Image acquisition and analysis was performed in the same method as previously described.

Measurement and analysis of BCR cluster growth

Naïve and GC B cells were isolated and sorted from tonsil, and their BCRs were labeled with Alexa Fluor 488 anti-IgM (Jackson ImmunoResearch) Fab for naïve B cells, or with Alexa Fluor 488 anti-IgG Fab (Jackson ImmunoResearch) for GC B cells. Time-lapse live cell TIRF imaging was performed at 37°C on a heated stage with 5% CO_2 gas supply and 75% humidity. Each B cell subset was placed on PLBs containing goat F(ab')$_2$ anti-human Igκ (SouthernBiotech) and goat F(ab')$_2$ anti-human Igλ (SouthernBiotech) surrogate antigen, and images were acquired at 3 sec intervals for 20 min. BCR cluster growth was measured by MatLab (MathWorks).

Measurement and analysis of Ezrin, SNX9, SNX18, LAMP-1 and surface VLA-4 and LFA-1 expression

Purified tonsillar B cells from five different individuals were stained with near-IR Live/Dead marker (ThermoFisher), DyLight 405 (Innova Biosciences) conjugated anti-IgD Fab (SouthernBiotech), BV786 anti-CD10 (BD Biosciences), PE anti-CD184 (BD Biosciences), Alexa Fluor 488 anti-CD29 (Biolegend), Alexa Fluor 647 anti-CD49d (Biolegend), DyLight 488 (Innova Biosciences) anti-VLA-4 active epitope (EMD Millipore), PE-Cy7 anti-CD11 (Biolegend), or FITC anti-CD18 (Biolegend) on ice, washed, and the amount of signal was quantified by flow cytometry (BD LSR II) and Flow cytometry data was analyzed with FlowJo (FLOWJO, LLC) and Prism (GraphPad) software.

For Ezrin, SNX9, SNX18, and LAMP-1 staining, purified tonsillar B cells from five individuals were stained with near-IR Live/Dead marker (ThermoFisher), DyLight 405 (Innova Biosciences) conjugated anti-IgD Fab (SouthernBiotech), BV786 anti-CD10 (BD Biosciences), PE anti-CD184 (BD Biosciences) on ice, washed, and stained cells were fixed and permeabilized using BD Cytofix/Cytoperm (BD Biosciences) following manufacturer's protocol. Stained cells were incubated with anti-Ezrin (Cell Signaling), anti-SNX9 (Sigma), anti-SNX18(Sigma), or DyLight 550 (Innova Biosciences) conjugated anti-LAMP-1 (Abcam) antibodies at room temperature for 2 h, washed. For Ezrin, SNX9, and SNX18, cells were stained with Alexa Fluor 647 secondary antibodies (Invitrogen), washed, and the amount of signal was quantified by flow cytometry (BD LSR II) and Flow cytometry data was analyzed with FlowJo (FLOWJO, LLC) and Prism (GraphPad) software.

VCAM-1 binding assay

30ul of Nickel Agarose magnetic beads (Sigma) were washed and incubated with either 100ug of recombinant human VCAM-1 Fc chimera proteins (R&D Systems) or purified human IgG (MP biomedicals) for 4 h in diH_2O containing 0.1% BSA, 50mM Tris-HCl pH 8.0, 10mM imidazole, and 100mM NaCl (washing buffer). They were then washed in HBSS containing 0.1% BSA, 10mM imidazole, 100mM NaCl (binding buffer). Negatively-isolated tonsillar B cells in binding buffer were mixed with nickel agarose magnetic beads and incubated on a tube rotator at 37°C for 30 min. Unbound cells were collected using a magnetic separation stand and bound cells were eluted with HBSS containing 150mM imidazole (Sigma) elution buffer after washing. Bound and unbound B cells, as well as a control that had not been incubated with beads, were stained on ice for 20 min using near-IR Live/Dead marker (ThermoFisher), FITC anti-IgD (Miltenyi), and BV421 anti-CD10 (BD Biosciences) and the amount of signal was measured by flow cytometry (BD LSR II) and Flow cytometry data was analyzed with FlowJo (FLOWJO, LLC) and Prism (GraphPad) software.

STED, SEM, and confocal microscopy

Cells were placed on PLBs containing goat $F(ab')_2$ anti-human Igκ (SouthernBiotech) and goat $F(ab')_2$ anti-human Igλ (SouthernBiotech) surrogate antigen at 37°C for 25 min, fixed in 4% PFA, and permeabilized in saponin. For super resolution images of F-actin structure in the immune synapse, cells were stained with Alexa Fluor 488 phalloidin (ThermoFisher) and images were acquired with STED microscopy (Leica). For immune synapse and z-stack images of F-actin and BCR, cells were labeled with Alexa Fluor 647 anti-IgM or anti-IgG Fab and were activated in the same manner as cells for STED images. Images were obtained using a Zeiss-880

confocal microscope and stacked images were deconvolved with Huygens Software (Huygens Software). For z-stack images of F-actin, ezrin, and BCR, LZ GC B cells were labeled with Alexa Fluor 647 anti-IgG Fab and were activated in the same manner as cells for STED images and images were obtained using a Zeiss-880 confocal microscope. The MFI and the Pearson's correlation coefficients of ezrin and F-actin were calculated from background-subtracted images by Zen software (Zeiss). For z-stack images of SNX9, SNX18, LAMP-1, and MTOC, naïve and LZ GC B cells were placed on PMS containing DyLight 650 (Innova Biosciences) conjugated goat $F(ab')_2$ anti-human Igκ (SouthernBiotech) and anti-human Igλ (SouthernBiotech) surrogate antigen and incubated at 37°C for 25 min or 45 min, and fixed in 4% PFA. Fixed cells were permeabilized in saponin and stained with Alexa Fluor 488 phalloidin (ThermoFisher), and anti-Ezrin (Cell signaling), anti-SNX9 (Sigma), anti-SNX18 (Sigma), anti-LAMP-1 (Abcam), anti-alpha tubulin, or anti-gamma tubulin at 4°C overnight. They were washed, stained with Alexa Fluor 550 secondary antibodies (Invitrogen), and washed. Images were obtained using a Zeiss-880 confocal microscope. Distance of MTOC, SNX9, and SNX18 cluster to PMS, and MFI and TFI of SNX9 and SNX18 per each z-stack were measured by ImageJ (NIH). 3D images and movies of SNX9, SNX18, LAMP-1 and colocalization of antigen with LAMP-1 were generated by Imaris (Bitplane).

For SEM images, cells were activated on PLBs coated with goat $F(ab')_2$ anti-human Igκ (SouthernBiotech) and goat $F(ab')_2$ anti-human Igλ (SouthernBiotech) surrogate antigen, or without antigen at 37°C for 25 min. Coverslip cultures were fixed in a 2.5% glutaraldehyde, 1% paraformaldehyde, and 0.1M sodium cacodylate buffer with a pH of 7.4. The coverslips were then rinsed in cacodylate buffer, post fixed with 1% OsO_4 in the same buffer, dehydrated in an ethanol series, and dried using a Samdri-795 critical point dryer (Tousimis Research Corp,

Rockville MD). The dried coverslip cultures were coated with 5nm of gold in an EMS 575-X sputter coater (Electron Microscopy Sciences, Hatfield PA) and imaged with a Hitachi S-3400 N1 scanning electron microscope (Hitachi High Technologies America, Inc., Pleasanton CA).

IRM

Time-lapse live cell TIRF IRM imaging was done at 37°C on a heated stage with 5% CO_2 gas supply and 75% humidity. Each B cell subset was placed on PLBs containing goat $F(ab')_2$ anti-human Igκ (SouthernBiotech) and goat $F(ab')_2$ anti-human Igλ (SouthernBiotech) surrogate antigen, and images were acquired at 3 sec intervals for 20 min.

MATLAB algorithms were developed to perform robust and automated image analysis to produce the following figures. We inverted the grayscale IRM signal in each image in order to positively correlate the proximity to the coverslip with the intensity values, and subtracted background. To measure the proximity to the coverslip from the center to the periphery of the area of interaction of naïve and LZ GC B cells, each cell was analyzed with the graph on the left representing the quantitative data of the naïve B cell and the one on the right corresponding to the quantitative data of the LZ GC B cell at 0, 10, and 15 min after BCR stimulation. We drew a radial line in each cell and analyzed the intensity over the length of that line for each time point. To quantify the membrane movement, we also inverted the grayscale IRM signal in each image in order to positively correlate the proximity to the coverslip with the intensity values above the background. After background subtraction, we calculated the change of mean fluorescence intensity of each cell. To count the contact sites of each cell, we ran another MATLAB algorithm that fits the image spots with modified Gaussian models. These modifications serve the purpose

of being able to recognize spots that aren't necessarily in the form of a PSF and captures more irregular shapes as long as they are a single 'spot.'

Detection and tracking of pod-like structures

For time-lapse live cell imaging, Igκ$^+$ naïve and LZ GC B cells were placed on PLB presenting anti-human Igκ or anti- rat Igκ antibodies surrogate antigens and incubated at 37°C on a climate-controlled stage with 5% CO_2 and 75% humidity, and DIC and IRM images were acquired at 3 sec intervals for 20 min. Movement of pod-like structures at early time point was measured for 3 min 45 sec from 2 min after activation and at late time point was measured for 8 min 45 sec from 11 min after activation on antigen-containing PLB. Analyses of time-lapse acquisitions were performed with MatLab and ImageJ. Pod-like structures from 3 LZ GC B cells exposed to high- or low-affnity antigen were analyzed and results were combined. First, any variations in intensity in DIC image sequences were normalized using linear regression in MatLab. Next, images were sharpened using an unsharp masking algorithm in MatLab to enhance the contrast of the pod-like structures. Pixels were next proportionately scaled down and binned into 8-bit unsigned integers to reduce the effects of small variations in pixel intensities. Masks were then created using a method similar to topographic prominence in ImageJ by iteratively applying the Maximum function to identify the local intensity maximum of pod-like structures as a single point. Points were then tracked over time and their diffusion coefficients calculated using Matlab code developed to track single particles.

Measurement and analysis of pulling forces

Goat F(ab')$_2$ anti-human Igκ (SouthernBiotech) and anti-human Igλ (SouthernBiotech) were conjugated to force and control sensors and used as surrogate antigen to measure sensor opening.

For the movies, images were background subtracted and flatfield corrected in ImageJ (NIH) and value 1000 was added to Atto550 images before ratio calculation to reduce background. For the statistical analysis, images were acquired after 20 min of incubation of the cells in antigen-containing PLB, background subtracted and flatfield corrected in ImageJ. Using the threshold function, the ratio of Atto647N to Atto550 fluorescence in antigen clusters of each cell was calculated by ImageJ and statistical analysis of sensor opening from each B cell subset was calculated by Prism software (Graphpad).

Antigen extraction and trafficking

To measure antigen extraction, PMSs were prepared as follows. Briefly, HEK293 cells were seeded onto poly-L-lysine coated chambers and cultured overnight in DMEM-10. Cells were washed and sonicated with a small probe at room temperature until their upper cell plasma membranes were removed. Sheared cells were then blocked in HBSS with 5% BSA and 2.5mM $CaCl_2$ at room temperature for 30 min, washed in a washing buffer of HBSS with 0.1% BSA, and incubated in washing buffer containing 50nM annexin V biotin (Biolegend). Cells were then washed, incubated in washing buffer containing 5ug/ml streptavidin (Sigma) for 30 min, washed, incubated in washing buffer containing either DyLight 550 (Innova Biosciences) conjugated anti-human Igκ antigen (GeneTex) or DyLight 550 (Innova Biosciences) conjugated anti-rat Igκ (ThermoFisher) surrogate antigen for 30 min, and washed again. Human tonsillar B cells were placed on PMSs and incubated at 37°C for 2 h. After incubation cells were harvested and stained with near-IR Live/Dead marker (ThermoFisher), DyLight 405 (Innova Biosciences) conjugated anti-IgD Fab (SouthernBiotech), BV786 anti-CD10 (BD Biosciences), and the amount of signal was quantified by flow cytometry (BD LSR II).

To measure antigen trafficking, PMSs were prepared in the same manner as in the antigen extraction experiment and additional pHrodo avidin (ThermoFisher) was added. Briefly, cells were incubated in washing buffer containing annexin V biotin, streptavidin, and biotin- and DyLight 650-conjugated goat $F(ab')_2$ anti-human Igκ (Southern Biotech) and goat $F(ab')_2$ anti-human Igλ (Southern Biotech) sequentially with washing steps after every incubation. They were then incubated in washing buffer with pHrodo avidin for 30 min and washed in washing buffer. Cells were placed on PMSs and incubated either at 37°C or on ice for the times indicated in the figure legends. For the control, irrelevant antigen pc-BSA labeled with biotin and Alexa Fluor 647 was used instead of antigen. After incubation, cells were harvested, stained with near-IR Live/Dead marker (ThermoFisher), DyLight 405 (Innova Biosciences) conjugated anti-IgD Fab (SouthernBiotech), BV786 anti-CD10 (BD Biosciences), and the amount of signal was quantified by flow cytometry (BD LSR II).

Activation of naïve and LZ GC B Cells and measurement of IRF-4 mRNA expression

To activate LZ GC B cells, PLBs were prepared as follows. Sorted $Igκ^+$ naïve and LZ GC B cells were placed on PLB presenting anti-human Igκ, anti- rat Igκ antibodies surrogate antigens or without antigen and incubated at 37°C on a climate-controlled stage with 5% CO_2 and 75% humidity for 1 h. Then the same volume of RPMI-10 culture media containing anti-CD40 antibody (2ug/mL, R&D systems), IL-4 (40ng/mL, R&D systems), IL-21 (2ug/mL Biolegend), or RPMI-10 culture media alone was added to LZ GC B cells, and cells were incubated at 37°C for an additional 2 h and harvested. LZ GC B cells were lysed, RNA was reverse transcribed, and cDNA was used to run TaqMan Gene Expression Assays using TaqMan Gene Expression Cells-to-C_T kit (ThermoFisher) on CFX connect Real-Time PCR Detection System (Bio Rad, check

model name again). TaqMan Gene Expression Assays detecting IRF-4 (Hs00180031_m1, ThermoFisher) and ACTB (Hs1060665_g1, ThermoFisher) were used to measure levels of mRNA and ACTB was used for normalization. Data were analyzed by Prism software (GraphPad).

Measurement and analysis of surface molecule expression

Purified tonsillar B cells from three different individuals were either incubated in RPMI-10 at 37°C for 2 h or incubated in RPMI-10 containing 10ug/ml of goat $F(ab')_2$ anti-human Igκ (SouthernBiotech) and anti-human Igλ (SouthernBiotech) and 5ug/mL of streptavidin (Sigma) at 37°C for 2 to establish a resting population and activated population, respectively. Cells were then washed and stained with Live/Dead marker (ThermoFisher), anti-CD19 (Biolegend), anti-IgD (Miltenyi), anti-CD10 (BD Biosciences), and anti-CD184 (BD Biosciences). Each population was then barcoded to differentiate the individuals and activation states, washed, combined, and further stained for surface markers of interest with LEGENDScreen (Biolegend) human cell screening kit as per the manufacturer's protocol. After completing the staining, cells were washed and fixed, and fluorescent signals were quantified by flow cytometry (BD LSR II). Flow cytometry data was analyzed with FlowJo v.10.1 and Microsoft Excel 2016. First, each of the six barcoded populations corresponding to the three individuals and two activation states were gated into $CD10^-$ IgD^+ Naïve, $CD10^-$ IgD^- Memory, and $CD10^+$ IgD^- GC B cell subsets. GC B cells were further separated into $CD10^+$ IgD^- $CXCR4^{high}$ Dark Zone and $CD10^+$ IgD^- $CXCR4^{low}$ Light Zone subsets. Geometric means for the surface markers of interest were calculated. To remove background due to unspecific binding, isotype readings from corresponding individuals with matching activation states were subtracted from barcoded

populations for which staining antibodies of identical species and class had been used. To ensure the validity of the following calculations, a floor was set to adjust background-corrected values that were negative or very small. The naïve B cell subset was used as a control with which we compared the other subsets, and a threshold requirement was set based on the absolute difference between the naïve background-corrected values and the background-corrected values of their other corresponding subsets to filter out false positives arising from small variations at low fluorescence intensities. The fold changes over naïve were then calculated for each subset and displayed as the binary logarithm transformations of these ratios.

Supplementary Materials:

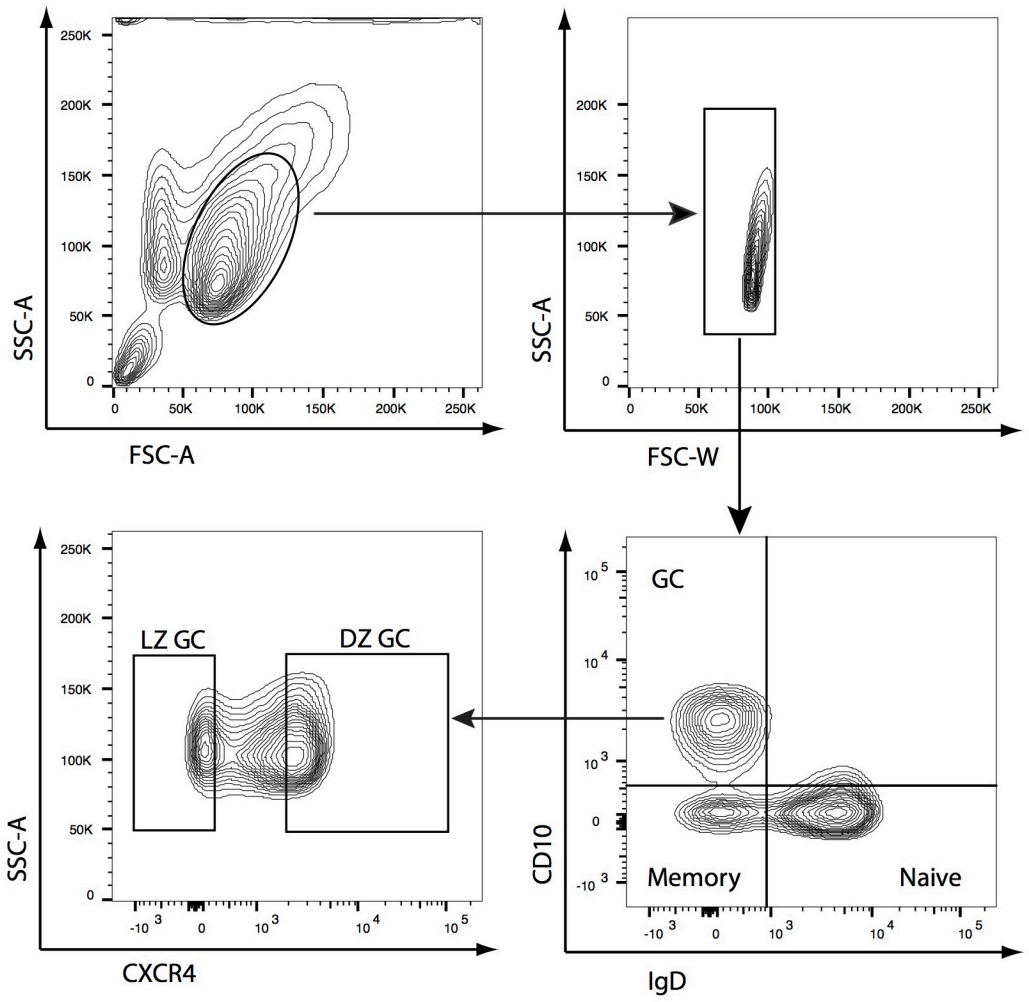

Fig. S1. FACS sorting gating strategy for naïve, memory, LZ GC, DZ GC B cells. To discriminate naïve, memory, and GC B cells, IgD and CD10 are plotted. To further discriminate LZ GC and DZ GC B cells from GC B cells, CXCR4 and SSC-A are plotted.

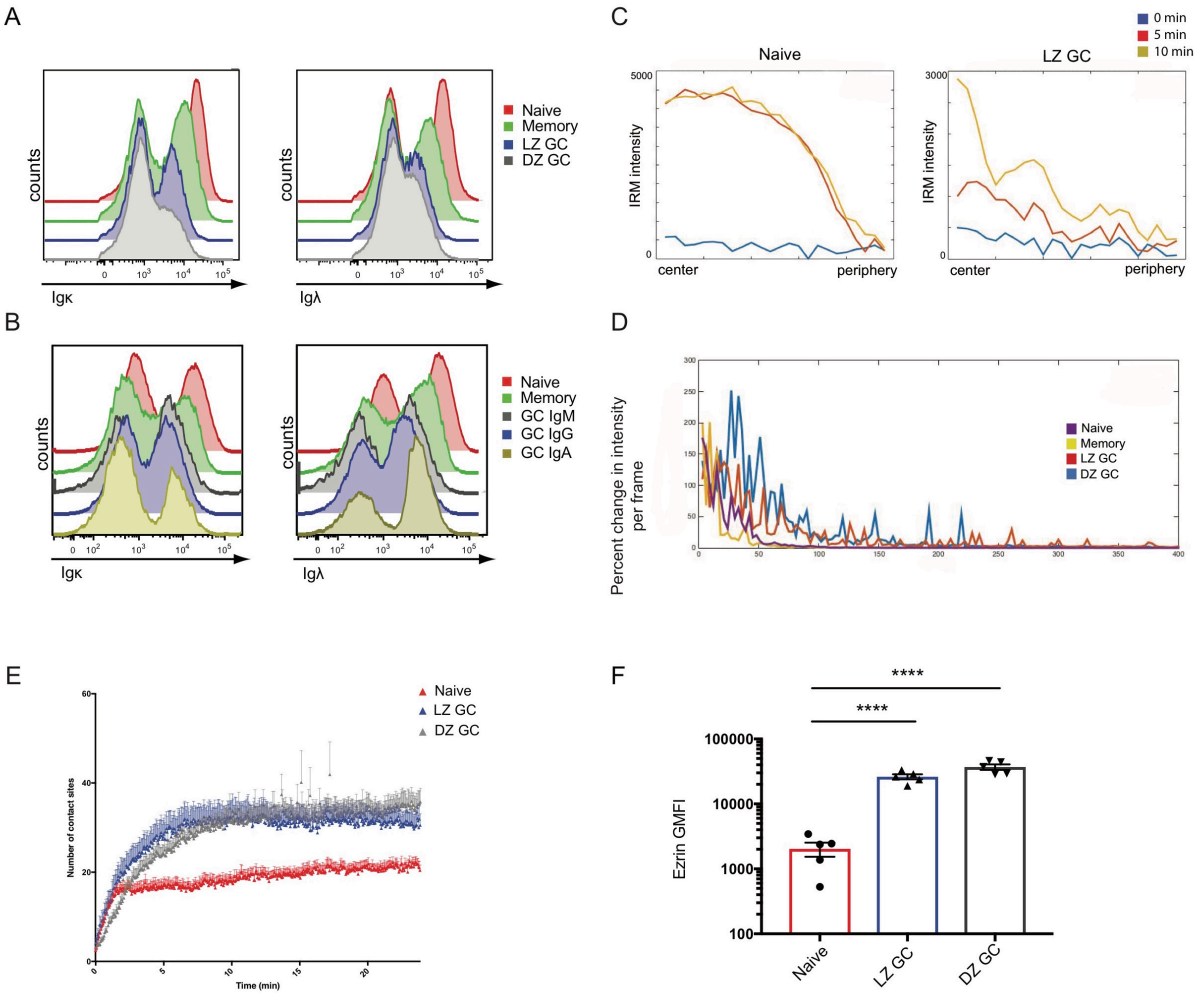

Fig. S2. Quantification of dynamic movement of unique pod-like structures formed in the immune synapse of LZ GC B cell and expression level of BCR and ezrin. (A) Surface expression of BCR on naïve B cells, MBCs, LZ GC B cells and DZ GC B cells measured by flow cytometry of B cells stained with fluorescent dye-conjugated anti-Igκ and anti-Igλ. **(B)** Surface expression of IgM, IgG, IgA BCRs on GC B cells, naïve B cells and MBCs as measured by anti-Igκ or anti-Igλ. **(C)** Proximity of cell membrane to PLB in the immune synapse as measured from the center to the periphery of the area of interaction after 0 min (blue), 5 min (red), or 10 min (yellow) of activation. **(D)** Membrane movement in immune synapses of B cell

subsets with time measured by quantification of change in intensity. **(E)** Counts of cell membrane contact sites of B cell subsets with time. Analysis methods are described in materials and methods. **(F)** The quantification of expression of ezrin in naïve, LZ GC, and DZ GC B cells by flow cytometry. *ns*>0.05, *$P \leq 0.05$, **$P \leq 0.01$, ***$P \leq 0.001$, and ****$P \leq 0.0001$ (unpaired *t*-test). Data are representative of three (A-B) or two experiments (C-D). (E-F: mean and s.e.m.)

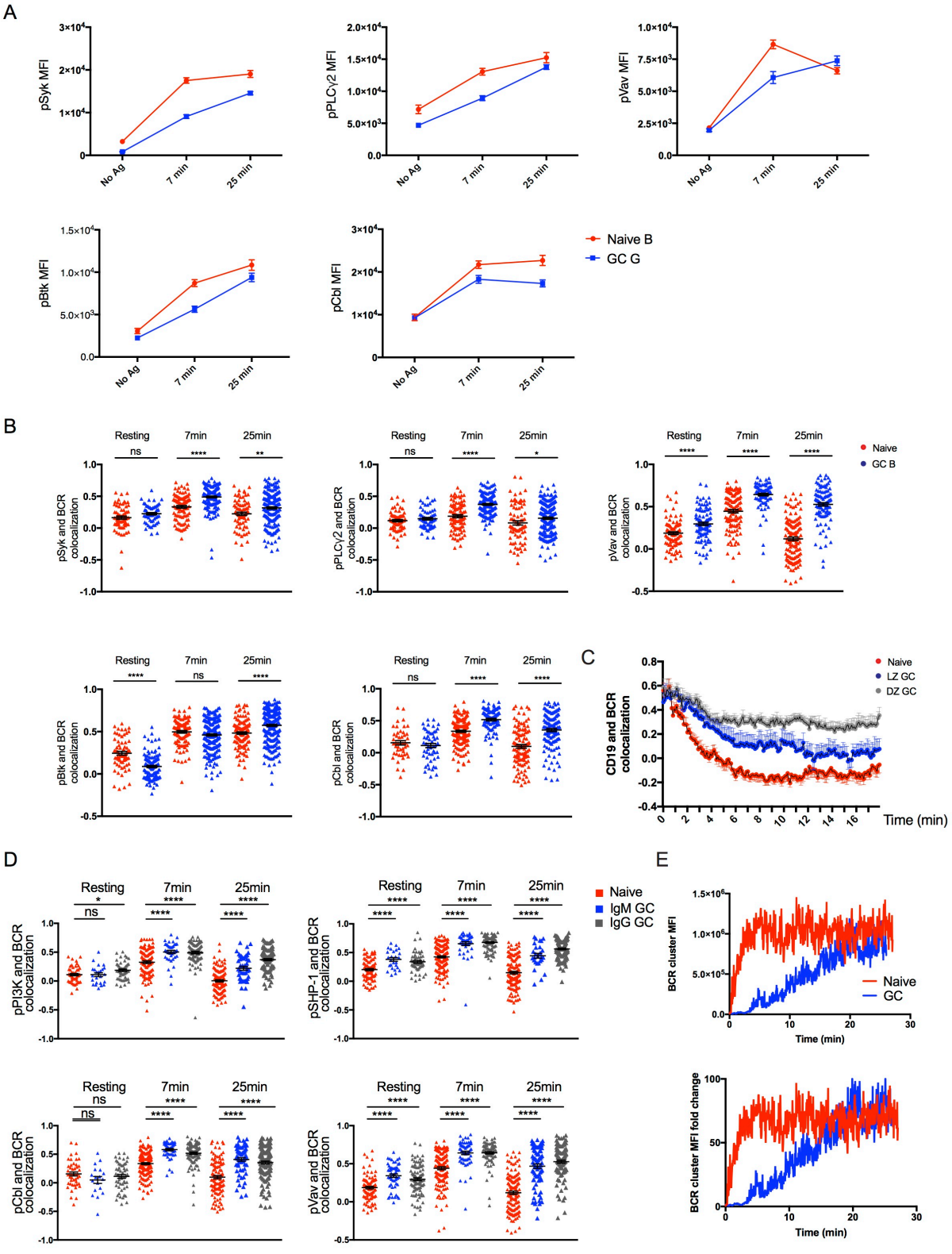
A
pSyk MFI
pPLCγ2 MFI
pVav MFI
pBtk MFI
pCbl MFI
No Ag
7 min
25 min
Naive B
GC G
B
Resting
7min
25min
pSyk and BCR colocalization
pPLCγ2 and BCR colocalization
pVav and BCR colocalization
pBtk and BCR colocalization
pCbl and BCR colocalization
Naive
GC B
C
CD19 and BCR colocalization
Naive
LZ GC
DZ GC
Time (min)
D
pPI3K and BCR colocalization
pSHP-1 and BCR colocalization
pCbl and BCR colocalization
pVav and BCR colocalization
Naive
IgM GC
IgG GC
E
BCR cluster MFI
BCR cluster MFI fold change
Time (min)

Fig. S3. Antigen-induced BCR signaling in naive B cells and GC B cells. (A) MFI of pSyk-1, pPLCγ2, pVav, pBtk, and pCbl in immune synapse of naïve and GC B cells. **(B)** Colocalization of BCR and pSyk-1, pPLCγ2, pVav, pBtk, or pCbl in immune synapse of naïve and GC B cells. **(C)** Colocalization of BCR and CD19 on live B cells with time on antigen-containing PLB as measured by quantification of TIRFM images (n= 8 per group). **(D)** Colocalization of BCR and pPI3K, pSHP-1, pVav, or pCbl in immune synapse of naïve B cells, IgM GC B and IgG GC B cells. **(E)** The growth of BCR cluster with time for naïve and GC B cells expressed as MFI of BCR labeled with Alexa Fluor 647-Fab anti-IgM for naïve B cells or anti-IgG for GC B cells (top panel) or fold change in the MFI of BCR clusters (bottom panel), measured as detailed in Materials and Methods (n=12 per group). *ns*>0.05, *$P \leq 0.05$, **$P \leq 0.01$, ***$P \leq 0.001$, and ****$P \leq 0.0001$ (unpaired *t*-test). Data are representative of two experiments. (A-D: mean and s.e.m.)

A

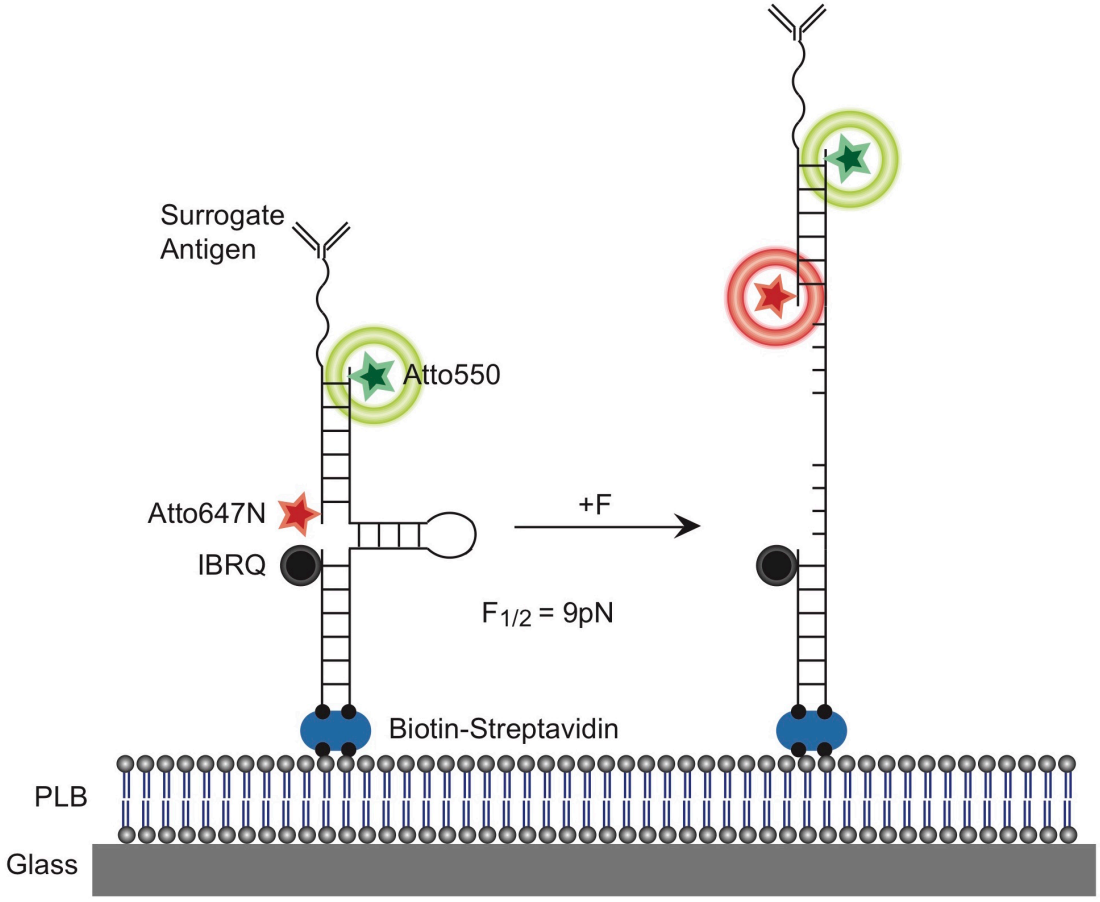
Surrogate
Antigen
Atto550
Atto647N
IBRQ
+F
F1/2 = 9pN
Biotin-Streptavidin
PLB
Glass

B

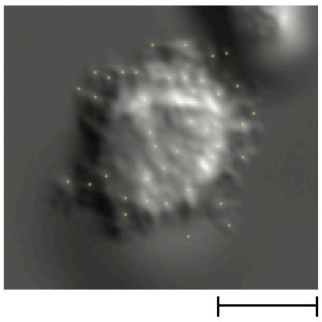

Fig. S4. Design of force sensor and detection of pod-like structures. (A) F(ab')2 anti-κ/λ as a surrogate antigen conjugated to a 9 pN DNA-based force sensor. **(B)** Detection of pod-like structures of LZ GC B cell placed on high-affinity antigen-containing PLB.

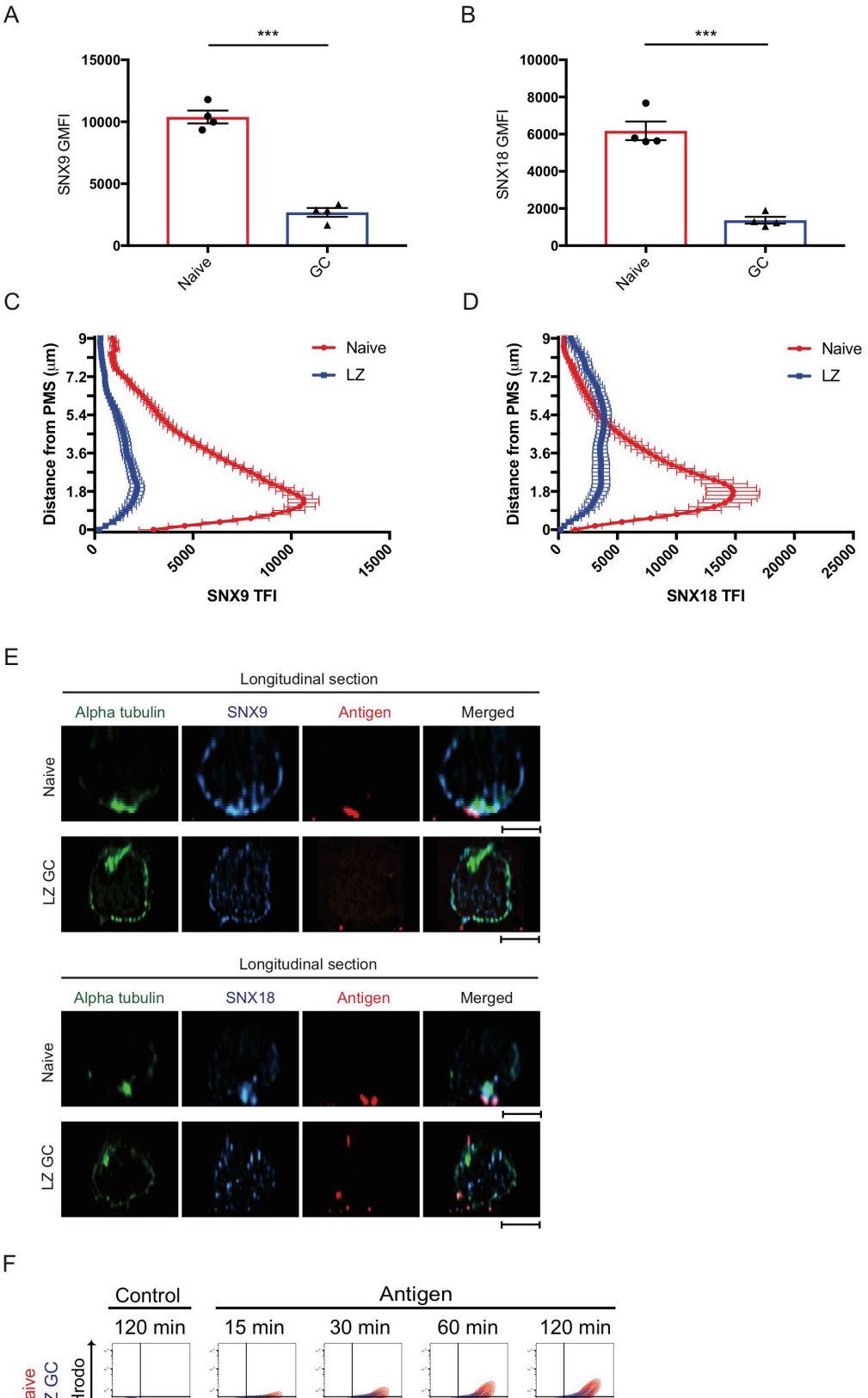
A
***
SNX9 GMFI
15000
10000
5000
0
Naive
GC
B
***
SNX18 GMFI
10000
8000
6000
4000
2000
0
Naive
GC
C
Distance from PMS (μm)
9
7.2
5.4
3.6
1.8
0
Naive
LZ
0
5000
10000
15000
SNX9 TFI
D
Distance from PMS (μm)
9
7.2
5.4
3.6
1.8
0
Naive
LZ
0
5000
10000
15000
20000
25000
SNX18 TFI
E
Longitudinal section
Alpha tubulin
SNX9
Antigen
Merged
Naive
LZ GC
Longitudinal section
Alpha tubulin
SNX18
Antigen
Merged
Naive
LZ GC
F
Control
Antigen
120 min
15 min
30 min
60 min
120 min
Naive
LZ GC
pHrodo
Antigen

Fig. S5. Polarization of SNX9 and SNX18 in naïve and LZ GC B cells after activation on antigen-containing PMS. (A-B) Quantification of SNX9 (**A**) and SNX18 (**B**) by flow cytometry. **(C-D)** Total fluorescence intensity (TFI) of SNX9 (**C**) and SNX18 (**D**) per each z-stack from the cell bottom to the top (n=25 per group). **(E)** Localization of SNX9 or SNX18 with MTOC in naïve and LZ GC B cells 45 min after activation on antigen-containing PMS. **(F)** Overlaid images of naïve B cells and LZ GC B cells. Scale bars are 5μm. *ns*>0.05, **P*≤0.05, ***P*≤0.01, ****P*≤0.001, and *****P*≤0.0001 (unpaired *t*-test). Data are representative of two experiments (E). (A-D: mean and s.e.m.)

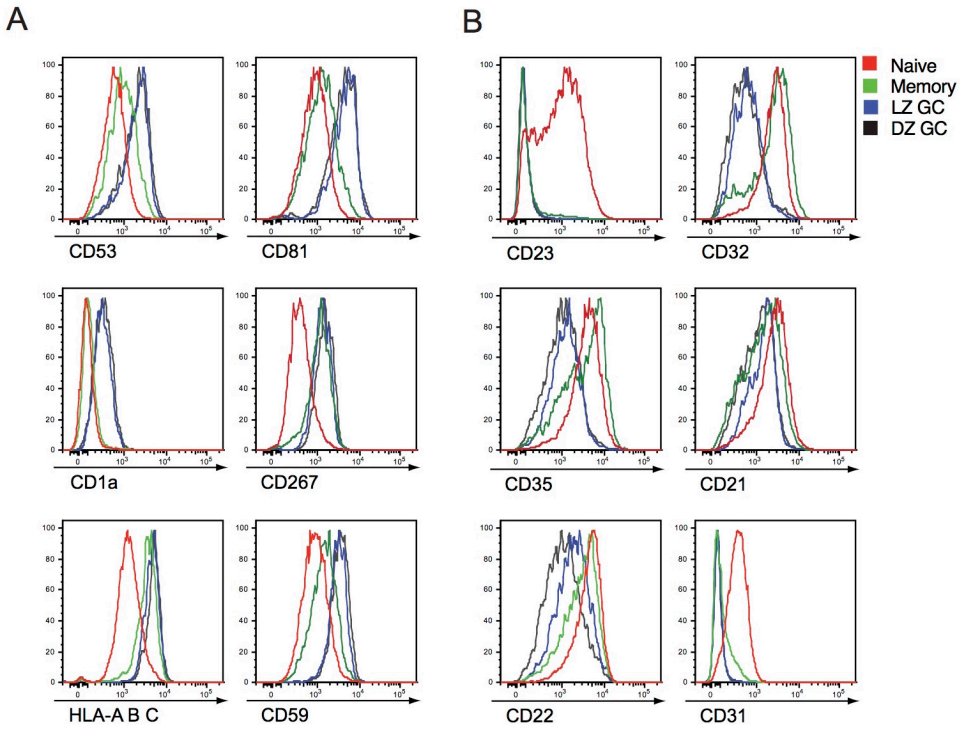
A
B
Naive
Memory
LZ GC
DZ GC
CD53
CD81
CD23
CD32
CD1a
CD267
CD35
CD21
HLA-A B C
CD59
CD22
CD31

C

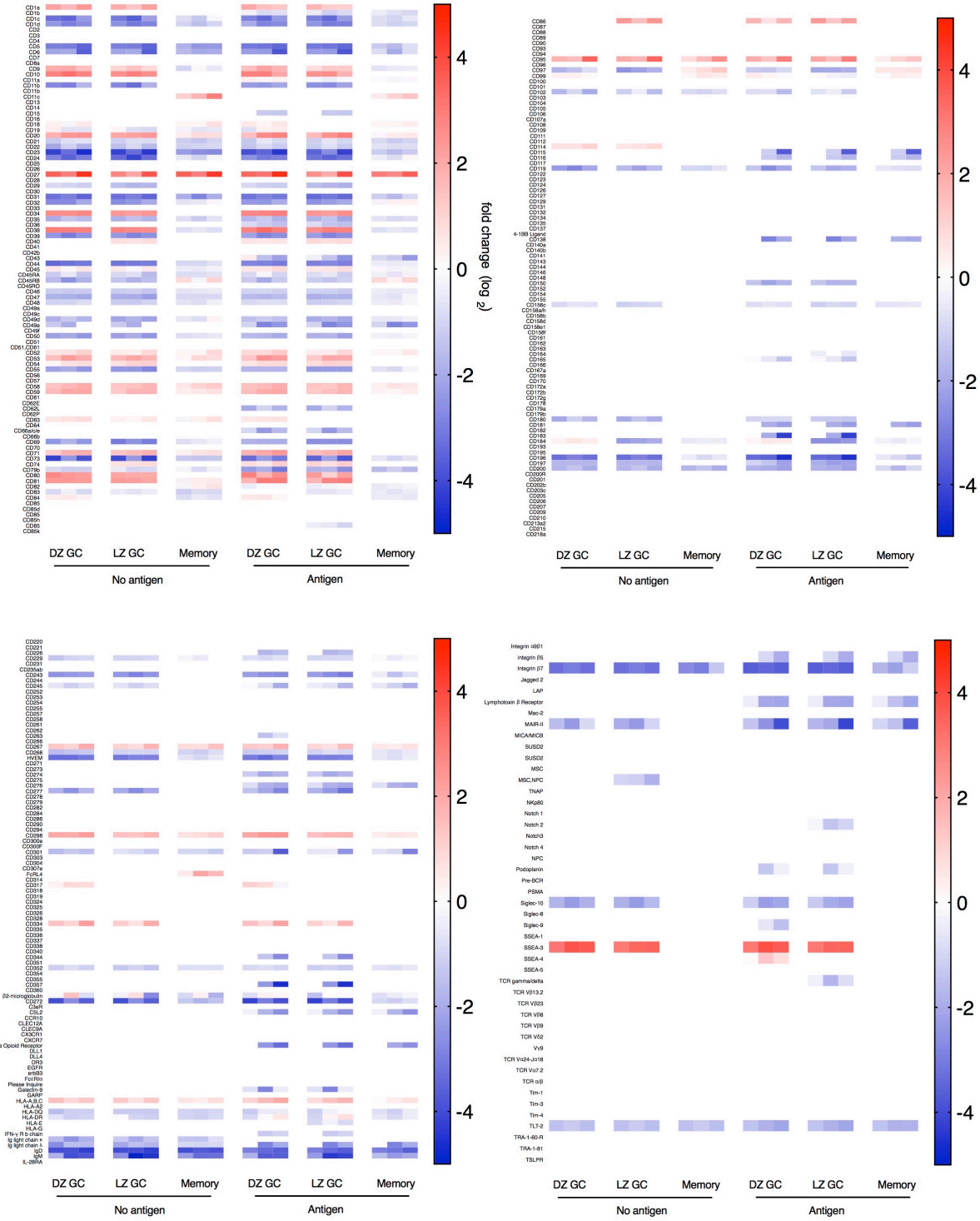
fold change (log 2)
4
2
0
-2
-4
DZ GC
LZ GC
Memory
DZ GC
LZ GC
Memory
No antigen
Antigen
DZ GC
LZ GC
Memory
DZ GC
LZ GC
Memory
No antigen
Antigen
DZ GC
LZ GC
Memory
DZ GC
LZ GC
Memory
No antigen
Antigen
DZ GC
LZ GC
Memory
DZ GC
LZ GC
Memory
No antigen
Antigen

Fig. S6. The Differential Expression of Key Surface Markers. (A) The cell surface expression level of CD53, 81, 1a, 267, HLA-A B C, and CD59 that are highly expressed on GC B cells. **(B)** The cell surface expression level of CD23, 32, 35, 21, 22, and 31 that are lowly expressed on GC B cells. (C) The surface expression level of total tested. Data are representative of three experiments (A and B).

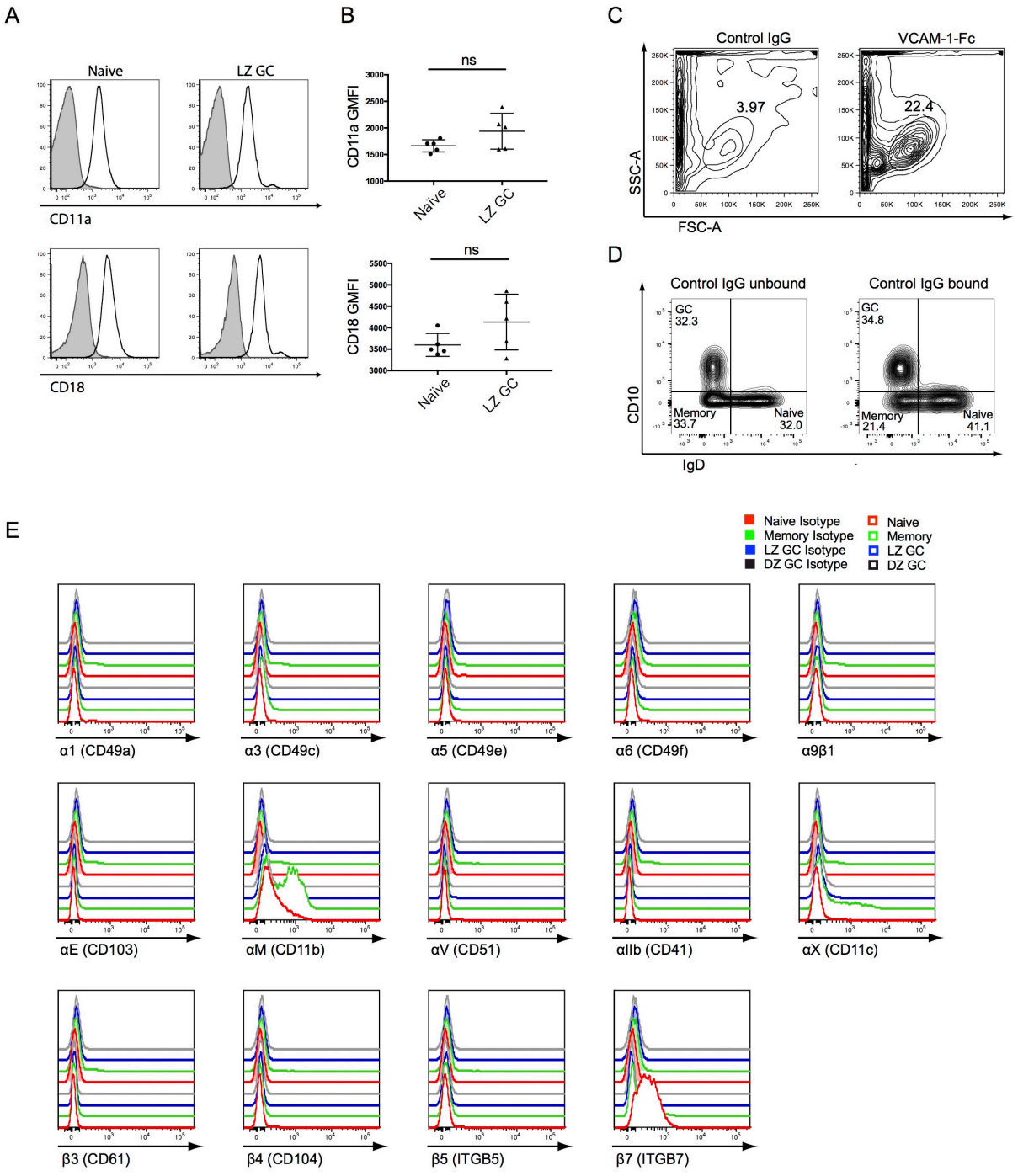

Fig. S7. Surface expression of LFA-1 and specificity of VLA-4 binding. (A-B) Surface expression level of CD11a and CD18 in naïve and LZ GC B cells. **(C)** Binding of B cells to

beads coated with VCAM-1 or Human IgG isotype 30 min after incubation. **(D)** Binding ability of naïve and GC B cells to beads coated with human IgG as a control. **(E)** Surface expression level of integrin molecules in naïve and LZ GC B cells. *ns*>0.05, *$P \leq 0.05$, **$P \leq 0.01$, ***$P \leq 0.001$, and ****$P \leq 0.0001$ (unpaired *t*-test). Data are representative of five independent experiments (A), three experiments (C-D), or three individuals (E). (B: mean and s.e.m.).

Movie S1. Distinctive membrane dynamics in the immune synapse of live naïve and LZ GC B cells placed on antigen-containing PLB were visualized by DIC (top panels) and IRM (bottom panels). Time-lapse imaging of naïve B cell (left panels) and LZ GC B cell (center panels) immune synapses upon activation, and LZ GC B cell (right panels) immune synapse without antigen.

Movie S2. The dynamics of membrane movement in the immune synapse upon activation were visualized by IRM. Time-lapse imaging of naïve B cell (top left), LZ GC B cell (bottom left), and DZ GC cell (bottom right) immune synapses upon activation on antigen-containing PLB was observed by IRM. The grayscale IRM signal in each image was inverted and colored by fire LUT in order to positively correlate the proximity to the coverslip with the intensity.

Movie S3. Time-lapse imaging of CD19 and BCR in the immune synapse of naïve B cells and LZ GC B cells. Naïve B cells and LZ GC B cells were activated by surrogate antigens presented on PLB and BCR (left panels, red) and CD19 (light panels, green) in the immune synapse of naïve (top panels) and LZ GC B (bottom panels) cells were imaged by TIRF.

Movie S4. Pulling forces in the immune synapse of live naïve and LZ GC B cells were monitored with time using DNA-based force sensors. The force-insensitive label Atto550 (green) and the force-sensitive label Atto647N (red) channels were merged (naïve: top left, LZ GC: bottom left) and the ratio of Atto647N/Atto550 defining sensor opening was calculated and visualized (naïve: top right, LZ GC: bottom right).

Movie S5. Colocalization of the cell contact sites and the locations of pulling force in LZ GC B cell. Signals from the force-insensitive label Atto550 (green) and the force-sensitive label Atto647N (red) were merged (top left), the ratio of Atto647N/Atto550 defining sensor opening was calculated and visualized (top right), The dynamics of membrane movement in the immune synapse were measured by IRM (bottom left), and sensor opening and IRM were merged (bottom right).

Movie S6. The dynamics of membrane movement in the immune synapse of naïve and LZ GC B cell upon activation by high- or low-affinity antigen were visualized by DIC (top panels) and IRM (bottom panels). Time-lapse live cell imaging of naïve B cell immune synapses activated by high-affinity (first panels) or low-affinity antigen (second panels) and LZ GC B cell immune synapses activated by high-affinity (third panels) or low-affinity antigens (fourth panels).

Movie S7. Motile LZ GC B cells were observed upon activation by low-affinity antigen. Time-lapse live DIC (left panel) and IRM (right panel) imaging of LZ GC B cell immune synapse activated by low-affinity antigen.

Movie S8. Distinct antigen transport pattern shown in human LZ GC B cells on PMS presenting surrogate antigens as compared to naïve B cells. Naïve (left) and LZ GC B cells (right) in 3D. Signals from DyLight633 conjugated goat $F(ab')_2$ anti-human Igκ and anti-human Igλ surrogate antigens (red) and F-actin (green) were acquired by confocal microscopy.

Movie S9. Localization of MTOC with SNX9 or SNX18 after activation in naïve and LZ GC B cells. Naïve (SNX9: top left, and SNX18: bottom left) and LZ GC B cells (SNX9: top right, and SNX18: bottom right) in 3D. Signals from DyLight633 conjugated goat $F(ab')_2$ anti-human Igκ and anti-human Igλ surrogate antigens (red), SNX9 or SNX18 (cyan), and alpha-tubulin (green) were acquired by confocal microscopy.

Movie S10. Localization of LAMP-1 after activation in naïve and LZ GC B cells. Naïve (left) and LZ GC B cells (right) in 3D. Signals from DyLight633 conjugated goat $F(ab')_2$ anti-human Igκ and anti-human Igλ surrogate antigens (red), F-actin (green), and LAMP-1 (cyan) were acquired by confocal microscopy.

Table S1. Raw data file